A single-cell-based model of multicellular growth using the immersed boundary method

Robert Dillon, Markus Owen, and Kevin Painter

Abstract. We present a single-cell based model for the growth and division of eucaryotic cells. The fluid-elastic structure of the cells and extracellular matrix are represented within the framework of the immersed boundary method. This is coupled with equations representing the diffusion and consumption of a nutrient. Numerical simulations of the model in the context of solid tumor growth and ductal carcinoma are presented.

1. Introduction

The growth processes of multicellular organisms and collections of cells such as bacterial colonies, though diverse, share the common features of individual cell growth and division. A variety of approaches have been taken to model multicellular growth, from continuum partial differential equation models for multicellular spheroids growth *in vitro* to a range of individual based approaches. PDE models have been used for many years to explore the coupled dynamics of cellular populations and biochemical substrates and regulators of proliferation and cell death. This includes relatively simple models for nutrient consumption in a tumor spheroid [**18**], and more complex models with mechanical effects [**7**], multiple interacting populations [**36**], and pattern formation on growing domains [**23**]. These approaches neglect the details of individual cell growth and movement. Perhaps the simplest individual based model is a cellular automaton in which each cell is represented by a single automaton location, and cell division and/or movement is determined by simple rules. Examples include their application to the migration of contact inhibited cells [**22**], and to cancer growth and its interaction with the immune system [**29**]. More advanced models include the so-called lattice-gas automata [**8**]. Other extensions to this approach include models that incorporate extracellular diffusible substances (e.g. nutrients), intracellular dynamics, such as for the cell cycle, via systems of ODEs that model the relevant regulatory networks, and coupling to other model layers such as a vascular network [**1, 5, 24**] or the extracellular matrix

2000 *Mathematics Subject Classification.* 92B05,92C50,76D05,76Z99.

Key words and phrases. immersed boundary method, growth of elastic cells, formation of solid tumors.

The research of R. Dillon has been supported in part by an NSF grant DMS-0109957.

KJP acknowledges partial support from NIH grant CA113004.

(which can mediate haptotaxis and invasion) [**2, 3**]. Probably the closest model in spirit to the immersed boundary model that we outline below is the Monte Carlo approach of Drasdo and co-workers, which treats cells as elastic sticky spheres with a hard center. This approach has been applied to a range of systems including monolayer and spheroid cultures [**13, 14**], and liver regeneration [**19**]. However, this approach does not explicitly include the fluid uptake that is required for cell growth. Rather, cell growth is dependent on the degree of cell packing, with no restriction if cells are not touching [**13**]. A hybrid model is presented in [**21**] in which the cells in the proliferating region of a tumor are represented by discrete deformable ellipsoidal cells while the remainder of the tumor is represented as a continuum. Again, the model for the growth of individual cells does not explicitly include fluid uptake. A multiscale model for avascular tumor growth is presented in [**20**] in which the cellular dynamics of proliferation and adhesion are described by means of a Monte Carlo model on a lattice (single cells are represented by a set of lattice sites), intracellular dynamics by means of a Boolean network that regulates the cell cycle, with reaction diffusion equations representing the chemical dynamics on the extracellular level. Here, cell growth and death do require uptake and release of volume: proliferating cells grow by invading lattice sites previously occupied by medium, and cell death is accompanied by a corresponding addition to the volume of the necrotic core.

We present here an immersed boundary model for multicellular growth in animal tissues. This model incorporates essential aspects of the mechanical forces involved in growth and cell division of individual cells, and in particular explicitly includes the fluid sources required for cellular volume changes. This is a significant advantage in this type of model since cell growth requires the uptake of both nutrients and fluid from the nearby extracellular space. Additionally, this approach provides the pressure and force distribution within the tissue and can be used for testing the influence of stress on cell proliferation and death.

The immersed boundary method, originally developed by Peskin for modeling the fluid mechanics of the heart [**25, 27**], provides a framework for coupling the dynamics of flexible boundaries with a viscous incompressible fluid. The method has been used to model a variety of phenomena involving fluid-structure interaction including aquatic animal locomotion [**16**], sperm and cilia motility [**10, 9**], platelet aggregation in the blood's clotting response [**17**], and three-dimensional blood flow in the heart [**28, 26**].

The immersed boundary method has been employed in the context of tissue growth in vertebrate limb development [**12**] and in the development of the villous trophoblast in the placenta [**33**]. In Section 2 we describe a cells-based immersed boundary model for tumor growth. An earlier version of this model without nutrient transport was briefly described in [**32**]. We shall refer to our model as (DOP). Rejniak [**30, 31**] has also developed a cells-based immersed boundary model for tumor growth which we shall refer to as (Rejniak). Although the two models (DOP) and (Rejniak) are similar in concept, there are important differences in the model details. In [**32**], the (DOP) and (Rejniak) models were both used in a study of ductal carcinoma and the differences between the two models were described in detail. In comparison with (Rejniak), the full (DOP) model presented in this work provides a more detailed description of the cell membrane and of the fluid channels that move fluid into the cell and provides a more accurate description of

the extracellular fluid transport. Both models include a simplified description of the extracellular matrix (ECM). The ECM mediates cell-cell adhesion. A second role in our model ECM is to maintain separation between cells. In a 2D model, separation between cells allows fluid transport in the extracellular space. In the (DOP) model we also incorporate a means for coupling the fluid/elastic equations with an advection, diffusion, reaction equation for nutrients in the extracellular space.

In the following sections, we present the mathematical framework for the immersed boundary model, a description of the numerical methods, as well as several simulations depicting solid tumor growth as well as the development of ductal carcinoma.

2. Mathematical model

The schematic of a model cell is shown in Figure 1(a). Each cell is modeled

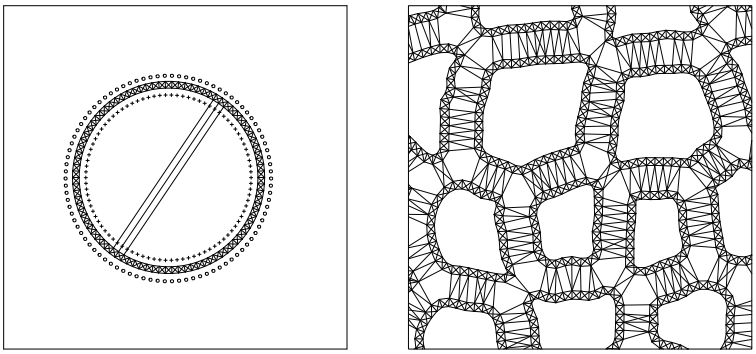

(a) (b)

FIGURE 1. (a) Schematic of model cell. The cell wall is represented as a mesh of linear elastic forces. The transport of fluid from the exterior to the interior is facilitated via discrete channels modeled as source (o) and sink (+) pairs. The contractile force links for cell division extend across the cell. (b) Simulation detail of cell to cell link structure.

as a viscous fluid with additional elastic forces representing the cell membrane. In this simplified model, the cell's interior has no additional structure other than that provided by the fluid viscosity. The material properties of the cell wall are modeled via a network of linear elastic springs. During the growth process, additional fluid is introduced into the cell's interior via discrete fluid channels located around the circumference of the cell. Each channel is modeled as a discrete source and sink. In animal cells a contractile ring of actin and myosin filaments contracts during during cleavage to form the two daughter cells. In our two-dimensional model, this process is modeled via elastic links which extend from a region on the cell wall to the opposite side of the cell. These links contract and create a "cleavage furrow". After this contraction, the cell is split into two daughter cells. The model incorporates a simplified representation of an extracellular matrix that consists of additional

elastic links between neighboring cells. These links mediate cell-cell adhesion and can also maintain a minimal separation distance between cells.

Mathematical Representation

We assume that the fluid density is constant, but since there is growth, the continuity equation takes the form

$$\nabla \cdot \mathbf{u} = S(\mathbf{c}, \mathbf{x}, t), \tag{1}$$

wherein $\mathbf{u}$ is the local fluid velocity. The fluid is regarded as incompressible. However, the growth of individual cells is regulated via a system of discrete source and sink pairs located near the cell walls. The contributions of these discrete source and sink pairs are included in the source term S. The growth term S may also depend on a nutrient or oxygen $\mathbf{c}$. We assume that the fluid motion is described by the Navier-Stokes equations with source S (see [**4**]) given by Equation 2

$$\rho \frac{\partial \mathbf{u}}{\partial t} + \rho(\mathbf{u} \cdot \nabla)\mathbf{u} = -\nabla p + \mu(\nabla^2 \mathbf{u} + \frac{1}{3}\nabla S) + \mathbf{F}, \tag{2}$$

together with Equation 1. Here ρ is the fluid density, p is the pressure, and μ is the fluid viscosity. The term $\mathbf{F}$ is the force density (force per unit area in two dimensions) that the cells and links exert on the fluid. The force density $\mathbf{F}$,

$$\mathbf{F} = \sum_i \mathbf{F}_{cell(i)} + + \sum_j \mathbf{F}_{link(j)} + \sum_k \mathbf{F}_{contractile(k)}, \tag{3}$$

is comprised of forces representing the elastic properties of cell membranes, cell-cell links and the contractile forces of cell division.

Cell model

The k^{th} cell wall at time t is modeled as a ring of elastic material with finite thickness represented by $\mathbf{X}^k(r, s, t)$ where r, s are curvilinear coordinates. A force per unit area $\mathbf{f}_{\mathbf{cell}(k)}(r, s, t)$ is defined at each point on the ring. This immersed boundary force is transmitted directly to the fluid and gives a contribution to $\mathbf{F}$ which we call $\mathbf{F}_{\mathbf{cell}(k)}$,

$$\mathbf{F}_{\mathbf{cell}(k)}(\mathbf{x}, t) = \int \mathbf{f}_{\mathbf{cell}(k)}(r, s, t)\delta(\mathbf{x} - \mathbf{X}^k(r, s, t))drds, \tag{4}$$

where $\delta(\mathbf{x})$ is the two-dimensional Dirac delta function and the integration is over the cell membrane. The Eulerian force densities $\mathbf{F}_{link}$ and $\mathbf{F}_{contractile}$ are obtained via similar integrations with the Lagrangian force densities $\mathbf{f}_{link}$ and $\mathbf{f}_{contractile}$ defined on the cells $\mathbf{X}^k$. In addition, we require that the cells $\mathbf{X}^k$ move at the local fluid velocity via the equation

$$\frac{\partial \mathbf{X}^k(r, s, t)}{\partial t} = \mathbf{u}(\mathbf{X}^k(r, s, t), t) = \int \mathbf{u}(\mathbf{x}, t)\delta(\mathbf{x} - \mathbf{X}^k(r, s, t))d\mathbf{x}. \tag{5}$$

Here, the integration is over the fluid domain.

As shown in Figure 1, the discretized cell wall consists of an inner and outer ring of equally spaced immersed boundary points, $\mathbf{X}_{i,j}$. Here $i = 1$ ($i = 2$) is the index of the outer (inner) ring and $j = 1, \ldots N$ is the index of the points on each ring. Force densities $\mathbf{f}_{i,j}$ are defined at each point $\mathbf{X}_{i,j}$ on the cell wall. The force density at index (i, j) consists of forces between adjacent points on the inner and outer ring, forces between neighboring points on the inner and outer ring, as well as forces between points on the outer ring and nearby points on the inner ring . For any neighboring immersed boundary points with indices given by $q = (i_1, j_1)$

and $r = (i_2, j_2)$, the force $\mathbf{f}_{qr}$ at the immersed boundary point $\mathbf{X}_q$ due to the elastic link with the immersed boundary point $\mathbf{X}_r$ is given by Hooke's Law

$$\mathbf{f}_{qr} = S_{cell}(||\mathbf{X}_r - \mathbf{X}_q|| - D_L)\frac{\mathbf{X}_r - \mathbf{X}_q}{||\mathbf{X}_r - \mathbf{X}_q||}, \tag{6}$$

where S_{cell} is the spring force constant and D_L is the spring resting length. We set $D_L = H/2$ where H is the fluid grid size. The force at $\mathbf{X}_r$ due to the link with $\mathbf{X}_q$ is given by $\mathbf{f}_{rq} = -\mathbf{f}_{qr}$. The force density $\mathbf{f}_q$ is the sum of link forces between $\mathbf{X}_q$ and its neighbors $\mathbf{X}_r$ as described above. The total force $\mathbf{f}_{cell} = (\mathbf{f}_q)$. The Eulerian force $\mathbf{F}_{cell}$ is assembled via a discrete version of Equation 4 using an approximate Dirac delta function shown below.

Cell growth

Cell growth is driven by the transport of fluid via the source/sink pairs shown in Figure 1. These consist of an inner ring of sources balanced with an outer ring of sinks. In each source/sink pair, the fluid introduced via the interior source is equal to the fluid lost in the external sink. Thus the source term S in Equation (1) has the form

$$S = \sum_{ij}(S_{ij}^{+} - S_{ij}^{-}). \tag{7}$$

Here, S_{ij}^{s} is the contribution of the j^{th} source ($s = +$) or sink ($s = -$) for the i^{th} cell and has the form

$$S_{ij}^{s}(\mathbf{x}, t) = \sum S_{ij}\delta(\mathbf{x} - \mathbf{X}_{ij}^{s}). \tag{8}$$

S_{ij} is the growth rate constant of the $(ij)^{th}$ source and sink located at $\mathbf{X}_{ij}^{s}$. The growth rate of the i^{th} cell is determined by the size of S_{ij}, as well as the number of source/sink pairs associated with the cell. In our numerical implementation, a source/sink pair is associated with each of the immersed boundary points in the cell's outer ring. Each source/sink pair lies on a line that is approximately normal to the cell membrane. Each source (sink) is located at a distance $0.5H$ from the inner (outer) ring, where H is the fluid grid size. Since the sink-to-membrane distance is much less than the resting length of the cell-cell links, the sinks usually fall in the extracellular space between cells. When cells are closely packed, there may be an overlap between the sinks of neighboring cells and a reduction in the effectiveness of the source/sink channel.

The source strength S_{ij} may depend upon the cell state and very small or zero in a quiescent cell, or large in a rapidly growing cell. Moreover, the growth rate constant may depend on the local nutrient or oxygen concentration level as well as the local cell-cell link configuration.

As a cell expands in the growth phase, the cell wall must also increase in length. This is accomplished in the numerical method, by periodically remeshing the boundary – a process that typically requires additional new immersed boundary points and the remeshing of the cell wall.

Cell division

After sufficient growth, a model cell begins the process of cell division by activating the contractile links of the cortical ring. Each contractile link is represented by an equation similar to Equation 6 with a zero resting length and spring force constant $S_{contractile}$. As shown in Figure 2, the contraction of these links causes the cell to pinch. When the contractile links reach a prescribed length, the cell is

split into two daughter cells. See the sequence in Figure 2. Here, we use a simple

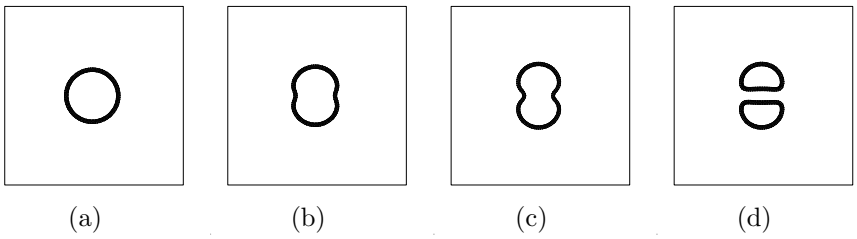

FIGURE 2. Simulation of cell division at the beginning (a), middle (b) , and end (c) of the division process. The two daughter cells are shown in (d).

model of the cell cycle in which cells begin the division process after reaching a prescribed size. The cells are split into two daughter cells when the length of the contractile links falls below a minimum length L_{min}. In our model implementation, the cell cycle may include additional phases such as a quiescent phase. However, in the simulations shown here, we eliminate the quiescent phase so that cells are either in a process of growth or cell division.

Cell-cell adhesion

Cell-cell and cell-wall adhesion are modeled by the creation of elastic springs or 'links' between immersed boundary points on the outer rings of the adherent cells with link stiffness S_{link}. The model for the formation and breakage of links is adapted from that used in [**15, 17, 11**] to model blood platelet and bacterial adhesion and aggregation. If the distance between immersed boundary points on different cells is less than a prescribed cohesion distance $D_{cohesion}$, an elastic link may be created between the two points to link the two cells. Detachment of cells is modeled by allowing the links to break when they are stretched beyond a prescribed length D_{break}. The link resting length $L_{resting}$ is also prescribed. Links between a cell and an immersed boundary wall such as the basal membrane included in simulations of ductal carcinoma (shown later) are created via a similar mechanism. The functional form of the cell-cell and cell-wall link forces is similar to the force shown above in Equation 6. In Figure 1(b) we show a detail of the cell and link structure. Additional details of the cell-cell and contractile links are given in [**32**].

Substrate kinetics and transport

Adding chemical dynamics to the model for cellular growth requires a solution to a system of reaction-diffusion-advection equations on an appropriate domain. Here we consider only extracellular chemicals (for example, nutrients or extracellular signaling molecules such as morphogens) and the regions inside cells are ignored. We denote by Ω_E the extracellular space.

To alleviate the numerical burden it is assumed that chemical dynamics are rapid on the timescale of cellular growth and that the contribution from advection due to fluid displacement is negligible. Therefore, at intervals much larger than the time step Δt required for solution of the Navier Stokes equations, we solve

$$0 = D_c \nabla^2 c + f(\cdot) \tag{9}$$

on the domain Ω_E. Boundary conditions will depend on the nature of the biological problem; for example, cells may either deplete a nutrient through uptake across

their membrane or secrete a signaling molecule into the extracellular space. To obtain a solution to the above equation, at each time step n we define Ω_E using the outer ring of the points for the cells (i.e. $\mathbf{X}_{1,q}$) . The *triangle* scheme of Shewchuk [**34, 35**] is used to perform Delaunay triangulation of the chemical grid. The nodes of the triangulation define the centers of tiles that form a Voronoi tessellation of Ω_E (see Figure 3). Each Voronoi tile V_i defines a control volume in a finite-volume-type

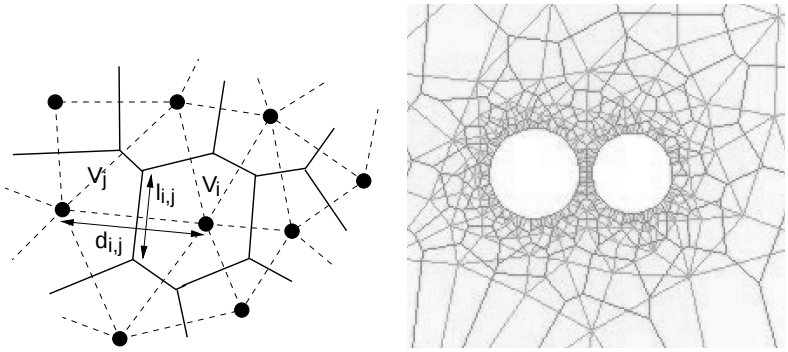

(a) (b)

FIGURE 3. (a) Illustration of Delaunay triangulation (dashed triangles) and the corresponding Voronoi tessellation (solid lines). (b) Detail of immersed boundary model showing two cells and the Delaunay triangulation.

scheme to approximate Equation (9) based on the method outlined in Bottino ([**6**]). Briefly, the Laplacian is approximated for each Voronoi tile V_i through summation of the fluxes across the faces partitioning V_i from each of its Delaunay neighbors,

$$\nabla^2 c_i \approx \frac{1}{A_i} \sum_{j \in N_i} \frac{c_j - c_i}{d_{i,j}} l_{i,j}$$

where c_i is the average concentration in V_i, A_i is the area of V_i, $d_{i,j}$ is the distance between the centers of V_i and V_j and $l_{i,j}$ is the length of the common edge between V_i and V_j. We obtain a solution to the steady-state Equation 9 by integrating the time dependent version of the spatially discretized equations forward in time until a steady state distribution is achieved to a sufficient degree of accuracy. Here we use a second order Runge-Kutta scheme for the reaction kinetics.

In our current numerical experiments, we assume the extracellular chemical is a nutrient. The feedback to the immersed boundary model for cellular growth is achieved by measuring the nutrient available to each cell. This is calculated here through surface integrals of the chemical concentration along each cell's membrane.

Numerical algorithm

The incompressible Navier-Stokes equations are solved in a domain of fluid within which the neutrally buoyant cells are immersed. Fluid quantities are represented on a grid (Eulerian description). Cell walls and links are modeled by discrete collections of moving points (Lagrangian description) connected by elastic links. The external force of an elastic object on the fluid is represented as a delta-function layer of force supported only by the region of fluid which coincides with

material points of the object as described in Equations 3; away from these points the external force is zero. The strength of this delta-function force is determined at each instant by the local configuration of the cells and links. The chemical concentration field is represented on a grid generated with a Delaunay triangulation. The size of the time step Δt required for the solution of the immersed boundary equations (1), (2), (4), and (5) is very small. Because of this, we solve for the steady state solution of the nutrient concentrations in Equation (9) less frequently and after every cell division.

The algorithm for the numerical solution of the model system may be summarized as follows: at the beginning of each time step n, we have the fluid velocity field $\mathbf{u}^n$, the configuration of the elastic boundaries $\mathbf{X}^n$, links, and the chemical concentration field c^n. In order to update these values we:

1. Calculate the force density $\mathbf{f}_{cell}$ from the cell configuration $\mathbf{X}^n$.
2. Update the cell-cell link structure.
3. Calculate the forces $\mathbf{f}^n_{link}$ imposed on the fluid by each link.
4. Calculate the forces $\mathbf{f}^n_{contractile}$ due to cells that are in the process of dividing.
5. Spread the force densities to the grid to determine the Eulerian force $\mathbf{F}$ on the fluid.
6. Spread the fluid source densities to the grid to determine the source strength S.
7. Solve the Navier-Stokes Equations 1 and 2 for $\mathbf{u}^{n+1}$.
8. Move the cells at the local fluid velocity in Equation 5 to obtain $\mathbf{X}^{n+1}$.
9. If a cell has completed the cell division process, solve Equation 9 for c^{n+1}.

A central feature of the immersed boundary method is that the immersed cells are not computational boundaries in the Navier-Stokes solver; they contribute a singular force field that alters the driving force in the fluid dynamic equations. We are therefore able to use a fluid solver designed for a regular grid with simple boundary conditions. For step (6) we use a method described in [**12**] for an incompressible fluid with distributed source and periodic boundary conditions. In steps (5), (6), and (8), we use a grid function to communicate information between the grid and the immersed objects. This is based on an approximate delta function of the form $\delta_h(\mathbf{x}) = d(x)d(y)$ where h is mesh width and

$$d(r) = \begin{cases} \frac{1}{4h}\left(1 + \cos\frac{\pi r}{2h}\right) & \mid r \mid < 2h \\ 0 & \mid r \mid \geq 2h. \end{cases} \tag{10}$$

We refer the reader to [**25**] for details. In the simulations shown below, the term $f(\cdot)$ in Equation 9 has the form

$$f(c) = -\alpha c \tag{11}$$

on the boundary of a cell. Away from the boundary, $f(c) = 0$.

In Figure 4 we show snapshots from a simulation of cell growth in order to illustrate the Delaunay triangulation and chemical concentration field. The dimensionless concentration scale is shown to the right of each panel. In these simulations, we use Dirichlet boundary conditions for the nutrient with $c = 1$ on the top and bottom and zero flux boundary conditions on the left and right edges of the domain. As shown in Figure 4 (left), two cells are placed in the center of the computational domain with the nutrient concentration field obtained by Equation 9. After each

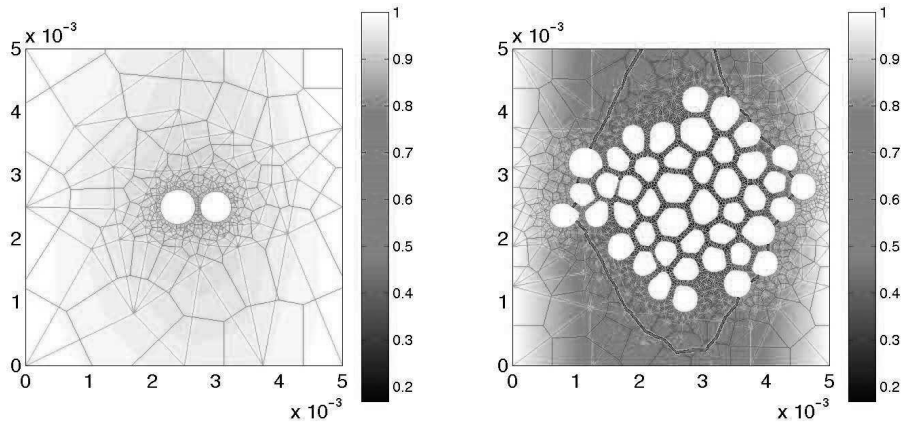

FIGURE 4. Cell growth simulation with chemistry.

cell division, we update the nutrient field concentration. The end of the simulation is shown in Figure 4 (right).

3. Numerical Simulations

In this section we present a preliminary set of numerical simulations for solid tumor growth, tumor growth with necrosis, and tumor growth in DCIS (ductal carcinoma in situ). In each simulation, the orientation of cell division is chosen to be approximately orthogonal to the cell's longest axis. The domain size for the tumor growth simulations is 0.04 x 0.04 cm^2. We use a 256 x 256 computational grid with a step size $\Delta t = 0.0012$s. For the solid tumor growth and tumor growth with necrosis simulations $D_{cohesion}$ and D_{break} are set to 0.00025 cm. In all cases, the link resting length $D_{resting} = D_{cohesion}$. We use a diffusion rate $D_c = 2 \times 10^{-5}$ cm^2/s, fluid density $\rho = 1$g/cm^3, fluid viscosity $\mu = 1000$g/(cm s), source strength $S_{ij} = 3 \times 10^{-5}$ g/cm, cell link stiffness $S_{cell} = 8 \times 10^4$ g/(cm s^2), cell-cell link stiffness $S_{link} = 5 \times 10^5$ g/(cm s^2), contractile force $S_{contractile} = 8 \times 10^5$ g/(cm s^2).

In the DCIS simulation the domain size is 0.02 x 0.02 cm^2 with a 256 x 256 computational grid. We use the same fluid density and viscosity as above with a step size $\Delta t = 0.0024$s, $D_{cohesion}$ and D_{break} set to 0.00025 cm, source strength $S_{ij} = 2 \times 10^{-5}$ g/cm, cell link stiffness $S_{cell} = 8 \times 10^4$ g/(cm s^2), cell-cell link stiffness $S_{link} = 5 \times 10^4$ g/(cm s^2), contractile force $S_{contractile} = 4 \times 10^5$ g/(cm s^2).

Solid tumor growth

In our model, the cell growth rate depends on the strength of the source strength S_{ij} in Equation 8. Here we consider three forms for the source strength equation

$$S_{ij} = S_0, \tag{12}$$

$$S_{ij} = S_0\, c_{ij}, \tag{13}$$

$$S_{ij} = max(S_0\, c_{ij}, .05\, S_0), \tag{14}$$

where S_0 is the uptake rate constant and c_{ij} is the local nutrient concentration at $\mathbf{X}_{i,j}$. In simulations governed by Equation 12, we do not solve Equation 9 since cell growth does not depend on nutrient concentration. According to Equation 11, nutrient depletion is due entirely to consumption by the individual cells. In this case, a key parameter in the reaction diffusion equation is the nutrient uptake or degradation rate parameter α seen in Equation 11. As seen in the simulations shown in Figure 4, a high nutrient uptake rate and increasing cell density can lead to a decrease in nutrient concentration c in the vicinity of the cells. Low nutrient concentration results in a slower cell growth rate via Equation 13.

In Figure 5 we compare the results of simulations with source given by Equation 14 and a (a) low nutrient uptake rate $\alpha = 0.001$, or (b) high nutrient uptake rate $\alpha = 0.01$. For comparison, we show in Figure 5(c) a simulation with source term given by Equation 12. We employ Dirichlet boundary conditions for Equation 9. The panels on the bottom row show a time/distance scatter plot of the cell division data. Time is shown on the x-axis and distance from the cell cluster centroid on the y-axis. In the simulations shown here, cell number increases with time and the maximum size is obtained at the end of the simulation. In the low nutrient uptake simulation in (a), the cell cluster reaches its maximum size after 56 days, whereas in the high uptake simulation in (b), the maximum size occurs after 183 days. In (c) the maximum size occurs at 129 days. The time scales shown in the scatter plots are adjusted so that the time on the right corresponds to the time at the end of the simulation. We use the term "day" as suggestive of the scaled time interval between consecutive frames. In simulations (a) and (b) there is a higher cell proliferation rate nearer the edge of the growing cell cluster. The cell proliferation rate in the more slowly growing cell cluster is relatively higher in the center of the cell cluster in comparison with the more rapidly growing cluster. The cell proliferation rate depends linearly on the local nutrient concentration. However, when the local nutrient concentration falls below a prescribed threshold, the cells maintain a constant growth rate. Different patterns (not shown) are obtained when the growth rates are governed by Equation 13. In that case, the cells furthest from the rim undergo very slow growth rates. Although the cell growth rates in (c) are independent of nutrient concentration, we still see a higher proliferation rate near the rim of the growing cell cluster.

Necrosis

In Figure 6 we show results from a set of simulations with "cell death". In this model of necrosis, a cell loses viability if the dimensionless average concentration of nutrient c at the cell boundary drops below a prescribed level c_{min}. In the simulations shown here, a cell is removed if the local cell concentration falls below c_{min}. We use Dirichlet boundary conditions for the nutrient in Equation 9 and, as a result, see some fingering develop as the rim of the cell cluster approaches the boundary. Since the dead cells are removed from the simulations, we are only seeing the viable proliferating cells. The width of this band of proliferating cells becomes narrower as the necrosis threshold level c_{min} is increased.

DCIS

In this section we show a pair of simulations representing the development of ductal carcinoma *in situ* or DCIS. Similar simulations of DCIS were presented in Rejniak and Dillon [**32**]. In each simulation, an outer ring representing the

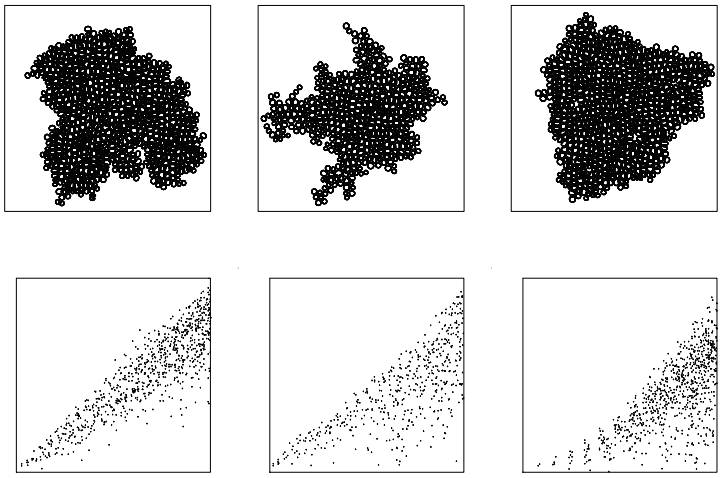

FIGURE 5. Top Row: Numerical Simulations of cell spheroid with nutrient uptake rate (a) 0.001 (785) (b) 0.01 (502) (c) uniform growth (793). The number of cells is shown in parentheses. Bottom Row: Scatter plots. The dots indicate the time (x-axis) and distance (y-axis) from the cell cluster centroid .

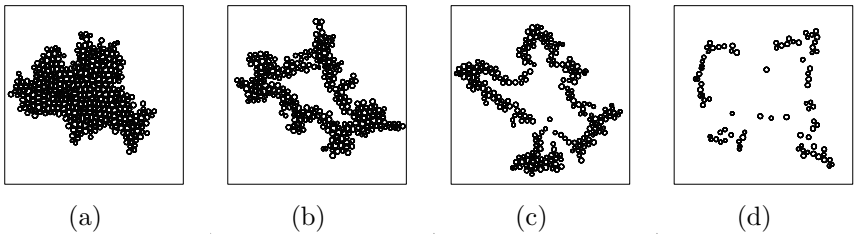

FIGURE 6. Simulations with necrosis at threshold levels c_{min} (at times) (a) 0.0 (166 days) (b) 0.00001 (166 days) (c) 0.0015 (180 days) (d) 0.05 (171 days). Here, the nutrient uptake rate is set to 0.01.

duct's basal membrane is represented as a set of immersed boundary points. The membrane's immersed boundary points are connected with elastic links and also tethered via stiff elastic links to fixed points in space . Initially, a ring of model cells is placed inside the duct and adjacent to the basal membrane. These cells represent the epithelial cells that line the duct. Normally, the growth and orientation of the epithelial cells is tightly regulated. However, in DCIS, a variety of growth patterns are seen. In Figure 7(top row) we show a cribiform pattern and in Figure 7 (bottom row), a solid pattern. In the solid pattern, a single cell and its daughter cells grow and divide in an unregulated fashion. The axis of cell division is determined randomly. In the cribiform pattern, a small number of epithelial cells are allowed to grow and divide. In this case, the axes of cell division are oriented radially so

that the cells form finger-like structures. In Figure 8 we show the completed solid

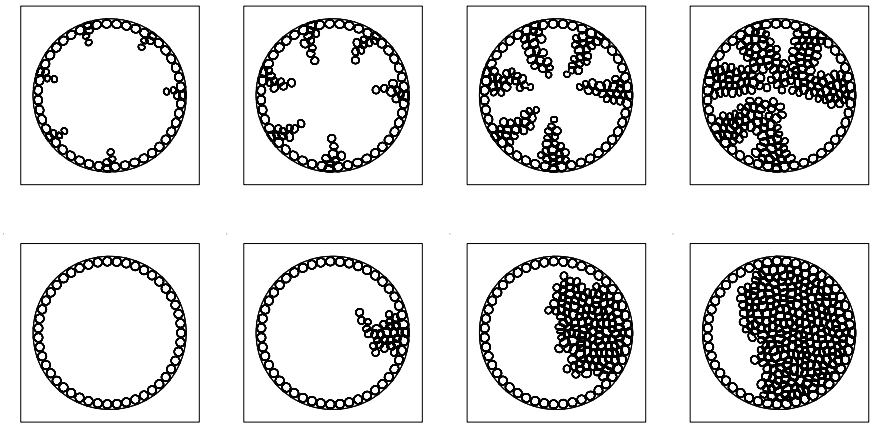

FIGURE 7. Tufting (top) and solid (bottom) patterns in DCIS

DCIS pattern.

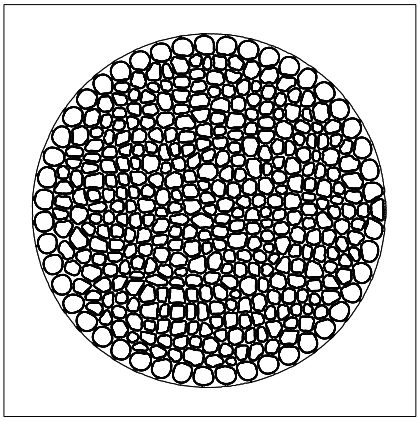

FIGURE 8. Solid pattern in DCIS

4. Discussion

In this paper we have presented a computational framework for the simulation of the growth and division of populations of biological cells using the immersed boundary method. A significant advantage of this approach is the explicit inclusion of the fluid contents of cells and the transport of fluid through the extracellular space. In order for cells to grow they must take up nutrients *and* fluid from the nearby extracellular space through specialized channels, which are modeled as source/sink pairs. A further advantage of this approach is the direct availability of

the pressure field and forces in the tissue, which would allow the testing of ideas about the influence of stress on cell proliferation and death. We have shown that this modeling framework is a natural way to consider individual cells in a growing tissue, and our simulations demonstrate the effects of nutrient depletion in growing clusters of cells, and a variety of morphologies that are consistent with those seen in ductal carcinomas.

We have included the dynamics of nutrients that diffuse in the extracellular medium by considering a quasi-steady reaction-diffusion equation at each time step. This assumes that the reaction and diffusion terms dominate over advection, although the uptake of fluid by growing cells results in an extracellular fluid flow which could in principle perturb the nutrient distribution. Therefore it is of interest to extend the nutrient calculations to include advection terms.

As well as animal tissues, this approach may have applications to plant cells. Here the details of cell growth are thought to include a balance between the turgor pressure in the vacuole of the cell and the mechanical properties of the cell wall. Here it may be important to be able to include different fluid properties in different regions, and osmotic effects. Addressing these issues would have further widespread applicability. Other model extensions could include ligand-receptor interactions at the cell-surface and subcellular signal processing. For example, a cell cycle module could be implemented as a set of ODEs associated with each cell, so that the spatial extent of the cell is neglected for simplicity. More detailed accounting for subcellular spatial structure is in principle straightforward, but would represent a significant computational challenge. Finally we note that these techniques carry over to three space dimensions, but with the obvious significant increases in computation time.

References

[1] T. Alarcon, H. M. Byrne, and P. K. Maini. A cellular automaton model for tumour growth in inhomogeneous environment. *J. Theor. Biol.*, 225(2):257–274, 2003.

[2] Alexander R. A. Anderson. A hybrid mathematical model of solid tumour invasion: the importance of cell adhesion. *Math. Med. and Biol.*, 22:163–186, 2005.

[3] Alexander R A Anderson, Alissa M Weaver, Peter T Cummings, and Vito Quaranta. Tumor morphology and phenotypic evolution driven by selective pressure from the microenvironment. *Cell*, 127(5):905–915, 2006.

[4] G. K. Batchelor. *An Introduction to Fluid Dynamics*. Cambridge, 1967.

[5] Russell Betteridge, Markus R. Owen, Helen M. Byrne, Tomás Alarcón, and Philip K. Maini. The impact of cell crowding and active cell movement on vascular tumour growth. *Networks and Heterogeneous Media*, 1(4):515–535, December 2006.

[6] D. C. Bottino. Computer simulations of mechanochemical coupling in a deforming domain: applications to cell motion. In P.K. Maini and H.G. Othmer, editors, *Mathematical Models for Biological Pattern Formation*, volume 121, pages 295–314. Springer-Verlag, New York, 2000.

[7] M A J Chaplain and B D Sleeman. Modelling the growth of solid tumours and incorporating a method for their classification using nonlinear elasticity theory. *J. Math. Biol.*, 31:431–479, 1993.

[8] Andreas Deutsch and Anna T. Lawniczak. Probabilistic lattice models of collective motion and aggregation: from individual to collective dynamics. *Math. Biosci.*, 156(1-2):255–269, 1999.

[9] R. Dillon, L. Fauci, C. Omoto, and X. Yang. Fluid dynamic models of flagellar and ciliary beating. *NYAS*, 1101:494–505, 2007.

[10] R. Dillon and L. J. Fauci. An integrative model of internal axoneme mechanics and external fluid dynamics in ciliary beating. *J. Theor. Biol.*, 207:415–430, 2000.

[11] R. Dillon, L. J. Fauci, A. Fogelson, and D. P. Gaver. Modeling biofilm processes using the immersed boundary method. *J. Comp. Phys*, 129:57–73, 1996.

[12] R. Dillon and H. G. Othmer. A mathematical model for outgrowth and spatial patterning of the vertebrate limb bud. *J. Theor. Biol.*, 197:295–330, 1999.

[13] D. Drasdo and S. Hohme. Individual-based approaches to birth and death in avascular tumors. *Mathematical and Computer Modeling*, 37(11):1163–1175, Jun 2003.

[14] Dirk Drasdo and Stefan Höhme. A single-cell-based model of tumor growth in vitro: monolayers and spheroids. *Physical Biology*, 2(3):133–147, 2005.

[15] L. J. Fauci and A. L. Fogelson. Truncated Newton methods and the modeling of complex immersed elastic structures. *Comm. on Pure and Appl. Math.*, 46:787–818, 1993.

[16] L. J. Fauci and C. S. Peskin. A computational model of aquatic animal locomotion. *J. Comp. Phys.*, 77:85–108, 1988.

[17] A. L. Fogelson. A mathematical model and numerical method for studying platelet adhesion and aggregation during blood clotting. *J. Comp. Phys.*, 56:111–134, 1984.

[18] H. P. Greenspan. On the growth and stability of cell cultures and solid tumors. *J. Theor. Biol.*, 56:229–242, 1976.

[19] Stefan Hohme, Jan G. Hengstler, Marc Brulport, Marc Schafer, Alexander Bauer, Rolf Gebhardt, and Dirk Drasdo. Mathematical modelling of liver regeneration after intoxication with ccl4. *Chemico-Biological Interactions*, 168(1):74–93, 2007.

[20] Y. Jiang, Jelana Pjesvivac-Grbovic, Charles Cantrell, and James P. Fryer. A multiscale model for avascular tumor growth. *Biophys. J.*, 89:3884–3894, 2005.

[21] Yangjin Kim, Magdalena A. Stolarska, and G. Othmer, Hans. A hybrid model for tumor spheroid growth *in vitro*: theoretical development and early results. *Math. Mod. Meth. Appl. S.*, 17:1773–1798, 2007.

[22] Y Lee, S Kouvroukoglou, L V McIntire, and K Zygourakis. A cellular automaton model for the proliferation of migrating contact-inhibited cells. *Biophys. J.*, 69(4):1284–1298, 1995.

[23] K. J. Painter, P. K. Maini, and H. G. Othmer. Stripe formation in juvenile Pomecanthus explained by a generalized Turing mechanism with chemotaxis. *PNAS*, 96:5549–5554, 1999.

[24] Aalpen A. Patel, Edward T. Gawlinski, Susan K. Lemieux, and Robert A. Gatenby. A cellular automaton model of early tumor growth and invasion: The effects of native tissue vascularity and increased anaerobic tumor metabolism. *J. Theor. Biol.*, 213(3):315–331, 2001.

[25] C. S. Peskin. Numerical analysis of blood flow in the heart. *J. Comput. Phys.*, 25:220–252, 1977.

[26] C. S. Peskin and D. M. McQueen. A three-dimensional computational model for blood flow in the heart i. immersed elastic fibers in a viscous incompressible fluid. *J. Comp. Phys*, 81:372–405, 1989.

[27] Charles S. Peskin. The immersed boundary method. *Acta Numerica*, pages 1–39, 2002.

[28] Charles S. Peskin and David M. McQueen. A three-dimensional computational method for blood flow in the heart. I. Immersed elastic fibers in a viscous incompressible fluid. *J. Comput. Phys.*, 81(2):372–405, 1989.

[29] An-Shen Qi, Xiang Zheng, Chan-Ying Du, and Bao-Sheng An. A cellular automaton model of cancerous growth. *J. Theor. Biol.*, 161(1):1–12, 1993.

[30] K. A. Rejniak. A single-cell approach in modeling the dynamics of tumor microregions. *Math. Biosci. Eng.*, 2:643–655, 2005.

[31] K. A. Rejniak. An immersed boundary framework for modelling the growth of individual cells: an application to early tumour development. *J. Theor. Biol.*, 247:186–204, 2007.

[32] K. A. Rejniak and R. H. Dillon. A single-cell based model of the ductal tumor microarchitecture. *Comput. Math. Meth. Med.*, 8:51–69, 2007.

[33] K. A. Rejniak, H. J. Kliman, and L. J. Fauci. A computational model of the mechanics of growth of the villous trophoblast bilayer. *Bull. Math. Biol.*, 66:199–232, 2004.

[34] J. R. Shewchuk. Triangle: Engineering a 2D Quality Mesh Generator and Delaunay Triangulator. In Ming C. Lin and Dinesh Manocha, editors, *Applied Computational Geometry: Towards Geometric Engineering*, volume 1148 of *Lecture Notes in Computer Science*, pages 203–222. Springer-Verlag, May 1996. From the First ACM Workshop on Applied Computational Geometry.

[35] J. R. Shewchuk. Refinement algorithms for triangular mesh generation. *Computational Geometry: Theory and Applications*, 22:21–74, 2002.

[36] Steven D. Webb, Markus R. Owen, Helen M. Byrne, Craig Murdoch, and Claire E Lewis. Macrophage-based anti-cancer therapy: Modelling different modes of tumour targeting. *Bull. Math. Biol.*, 69:1747–1776, 2007.

Department of Mathematics, Washington State University, Pullman, WA 99164, U.S.A
E-mail address: dillon@math.wsu.edu

Centre for Mathematical Medicine and Biology, School of Mathematical Sciences, University of Nottingham, Nottingham NG7 2RD
E-mail address: Markus.Owen@nottingham.ac.uk

School of Mathematical and Computer Sciences, Heriot-Watt University, Edinburgh, EH14 4AS, UK
E-mail address: painter@ma.hw.ac.uk